# Role of local heating in crystallization of amorphous alloys under ball milling: An experiment on $Fe_{90}Zr_{10}$

Y. S. Kwon and J. S. Kim
*Research Center for Machine Parts and Materials Processing, University of Ulsan, Namgu Mugeo 2-Dong, San 29, Ulsan 680-749, Korea*

I. V. Povstugar* and E. P. Yelsukov
*Physical-Technical Institute, UrB RAS, 132 Kirov Street, 426000 Izhevsk, Russia*

P. P. Choi
*Nano-Materials Research Center, Korea Institute of Science and Technology, P.O. Box 131, Cheongryang, Seoul 130-650, Korea*
(Received 2 October 2006; revised manuscript received 8 December 2006; published 25 April 2007)

$Fe_{90}Zr_{10}$ was chosen as a model system to elucidate the roles of mechanical deformation and local heating in the phenomenon of ball-milling-induced crystallization of amorphous alloys. The structural evolution of melt-spun amorphous $Fe_{90}Zr_{10}$ ribbons under different milling conditions and high-pressure torsion was investigated by means of x-ray diffraction, Mössbauer spectroscopy, and magnetic measurements. Despite a considerable difference in the local temperatures for high-energy and low-energy ball millings, cryomilling (under liquid nitrogen-cooling), and high-pressure torsion, amorphous $Fe_{90}Zr_{10}$ crystallizes into a supersaturated $\alpha$-Fe(Zr) solid solution in all cases. Local heating occurring under high- and low-energy millings only plays a minor role and leads to a slight shift of the crystallization products towards equilibrium state. Mechanical deformation was established as the primary cause of crystallization of the amorphous Fe-Zr alloy under ball milling.

DOI: 10.1103/PhysRevB.75.144112 PACS number(s): 81.05.Kf, 81.20.Wk, 81.10.Jt, 82.80.Ej

## I. INTRODUCTION

Mechanical alloying, i.e., ball milling of elemental or intermetallic powder mixtures, is a well-known process for producing a wide range of novel materials with unique properties. Particular interest has been paid in the past few decades to the formation of amorphous alloys by high-energy ball milling.[1–3] Several mechanisms have been proposed to explain the phenomenon of milling-induced amorphization.[4–6]. However, some amorphous alloys were found to undergo the "reverse" process under ball milling, namely, milling-induced crystallization (MIC).[7–11]

Despite numerous investigations of the phenomenon and mechanisms of MIC, its origin is still surrounded by controversy. Bansal *et al.*[7] ascribed the crystallization of a $Fe_{78}B_{13}Si_9$ metallic glass to impurity incorporation during milling, but more thorough studies have shown that MIC in a number of alloys also proceeds in the absence of impurities.[8] In general, MIC is considered to be a result of two simultaneous processes occurring under ball milling, namely, mechanical deformation and local heating of a material under colliding balls. Local temperature rises during high-energy ball milling can be up to several hundred degrees[12,13] and should therefore be taken into account when investigating the crystallization process. The influence of the external temperature on crystallization of a $Fe_{78}B_{13}Si_9$ amorphous alloy under milling in a vibrating-frame grinder, where global heating of the sample due to milling itself does not exceed 1 °C, was clearly demonstrated in Ref. 10. However, crystallization products obtained under ball milling are often found to be in a nonequilibrium state and strongly differ from those obtained under conventional thermal annealing,[8,14] clearly indicating that the MIC phenomenon cannot be solely ascribed to local heating effects.

As the local pressure generated by ball collisions in mills was estimated to amount up to 4–6 GPa,[15] the influence of similar hydrostatic pressure (several gigapascals) on the crystallization process at elevated temperatures was studied using Bridgeman anvils[16,17]. Nonequilibrium crystallization products were found under such a treatment, and it could be established that an increase in pressure results in a decrease in temperature of thermal crystallization. Deformation-induced crystallization of several Al-based metallic glasses was observed in shear bands resulting from bending.[14,18] Although temperature rise in shear bands can reach up to a few thousand degrees over a few nanoseconds,[19] such a time interval is extremely short for the formation of nucleation centers. Thus, crystallization of amorphous alloys can be solely induced by mechanical deformation under certain conditions.

To date, the fundamental question about the role of local heating effects in milling-induced crystallization still remains unanswered, i.e., whether local heating can be considered as the primary reason for MIC (while mechanical deformation just disorders crystallization products) or heating plays a minor role in a truly deformation-induced crystallization process. Since there is no reliable experimental technique for measuring the local temperatures in mills, it is challenging to investigate the role of local heating effects in the MIC process. Careful comparative analysis of the crystallization process and products obtained under different milling conditions, thermal treatments, and intensive low-temperature deformations appears to be a promising way of answering the question. Amorphous Fe-Zr was chosen as a model system in this work, as it attracted a great deal of attention in the

 

last decades[8,20–26] and a large amount of experimental data is available for this system. The composition of $Fe_{90}Zr_{10}$, where a single-phase amorphous state can be obtained using rapid quenching technique[24,25] but is unachievable under ball milling,[22] has been chosen.

In this work, $Fe_{90}Zr_{10}$ amorphous ribbons were ball milled under different milling conditions (high- and low-energy millings, cryomilling under liquid-nitrogen cooling). The samples after treatment were analyzed by means of x-ray diffraction (XRD), Mössbauer spectroscopy, and magnetic measurements. The results were compared with those obtained for $Fe_{90}Zr_{10}$ ribbons after high-pressure torsion deformation, which is a low-temperature process.

## II. EXPERIMENT

Initial ingots of $Fe_{90}Zr_{10}$ composition were prepared by arc-melting under high-vacuum conditions and subsequently melt spun to amorphous ribbons of about 5 $\mu$m in thickness with a single roller unit under Ar atmosphere. The melt-spun ribbons were cut into pieces of less than 1 cm in length and were mechanically treated in three different mills:

(i) High-energy milling was performed with an AGO-2 planetary ball mill, using vials and balls made of stainless steel. A ball-to-ribbon weight ratio of 40:1, a rotation speed of 1000 rpm (power intensity $>15$ W/g), and an external water cooling were chosen.

(ii) Low-energy milling was performed with a Pulverizette-7 planetary ball mill, using vials and balls made of hardened ball-bearing steel. A ball-to-ribbon weight ratio of 14:1, a rotation speed of 730 rpm (power intensity of 3.0–3.5 W/g), and an external air cooling were chosen.

(iii) A vibration ball mill was applied with vials and balls made of hardened ball-bearing steel. A ball-to-ribbon weight ratio of 12:1, a power intensity of 3 W/g, and an external cooling of the vial with liquid-nitrogen (cryomilling experiments) were chosen.

All milling experiments were performed in protective Ar atmosphere. The relative contamination of samples resulting from the debris of the milling tools was $<1\%$ in all cases, as measured by gravimetric analysis.

High-pressure torsion experiments were performed using a Bridgman anvil at an applied pressure of 8 GPa. Ribbon pieces of 3–4 mm in length were used for each experiment, varying the number of turns from 1/4 to 15. Each turn was performed slowly and lasted for 1 min, keeping a good thermal contact between the sample and anvil. Therefore, sample heating was negligible.

Structural characterization of the samples was performed by means of XRD using Cu $K\alpha$ radiation (wavelength of 0.154 06 nm). Mössbauer spectra were measured at room temperature using a spectrometer with a $^{57}$Co(Cr) source operating in constant acceleration mode. A generalizing regular algorithm for the solution of the inverse problem[28] was used to find hyperfine field distribution functions $P(H)$. The saturation magnetization was measured at room temperature using a vibrating-sample magnetometer in an external magnetic field of 16 kOe.

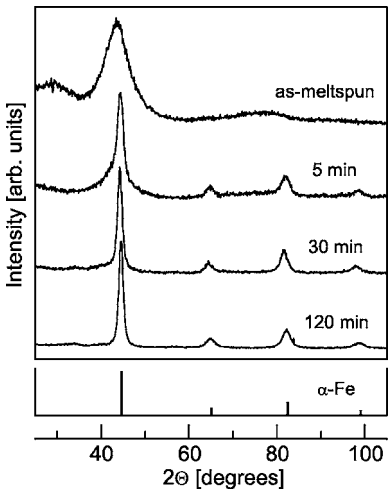


FIG. 1. XRD patterns of as-melt-spun ribbons and samples milled for various times (high-energy milling in AGO-2). The standard XRD pattern of pure a-Fe is shown below.

## III. RESULTS

### A. Crystallization under high-energy ball milling in AGO-2

The XRD pattern of the initial melt-spun ribbons shows (Fig. 1), besides a broad halo around 30° arising from the sample holder, a halo peak at 45° without any traces of crystalline phases, indicating a fully amorphous structure of the initial ribbons. Upon ball milling, crystallization of the amorphous phase takes place, and the formation of a bcc crystalline phase, having lines close to $\alpha$-Fe but shifted to lower angles, can be detected. Hence, $Fe_{90}Zr_{10}$ ribbons crystallize into a $\alpha$-Fe(Zr) solid solution, with a maximum Zr concentration of 2.8 at. % according to Vegard's law, which the is in good agreement with the results obtained by Trudeau.[8] The equilibrium Zr solubility in $\alpha$-Fe at room temperature is less than 0.1 at. %. Therefore, the formed solid solution is strongly supersaturated with Zr. From x-ray peak broadening, the average grain size of the solid solution was estimated to be lower than 20 nm for all samples. The XRD patterns of the milled samples do not reveal any pronounced peaks belonging to other phases such as intermetallics. Only diminishingly low and negligible peaks can be detected around $2\Theta$ angles of 34°, 40°, and 56.5°, which cannot be assigned to $\alpha$-Fe(Zr) nor to any oxide or nitride phases. They are assumed to belong to some metastable phase, possibly to the disordered $\phi$-$FeZr_2$ phase.[22] The crystallization proceeds with increasing milling time, as can be seen by the increasing intensities of the bcc peaks and peak sharpening. After 30 min of milling, no traces of the initial amorphous halo can be observed in the XRD patterns. The transformation of amorphous $Fe_{90}Zr_{10}$ into a nanocrystalline $\alpha$-Fe(Zr) solid solution virtually ends after 30 min of milling.

The XRD pattern of 120 min sample shows only peaks corresponding to bcc $\alpha$-Fe(Zr) solid solution, without any traces of other Zr-containing phases. As the maximum concentration of the solid solution is three times lower than the overall Zr content in the alloy, residual Zr is located in thin grain-boundary clusters or interlayers, being undetectable by

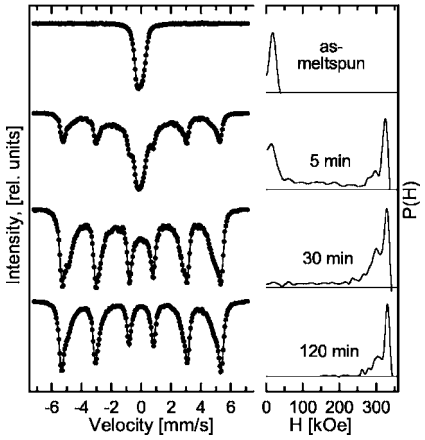


FIG. 2. Mössbauer spectra and corresponding hyperfine magnetic-field distribution functions of samples milled for various times (high-energy milling in AGO-2).

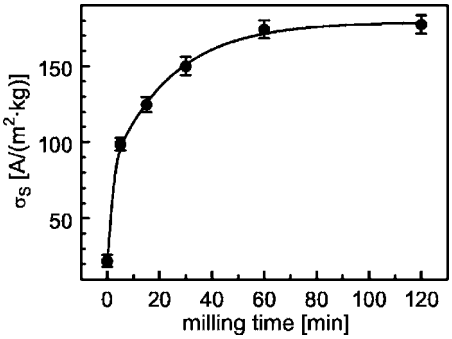


FIG. 3. Saturation magnetization plotted against the milling time (high-energy milling in AGO-2).

means of XRD. The effect of similar grain-boundary segregation was earlier observed under mechanical alloying in a set of Fe-based systems[29,30]. Thus, MIC of $Fe_{90}Zr_{10}$ amorphous alloy leads to the formation of supersaturated $\alpha$-Fe(Zr) solid solution with grain-boundary Zr segregations.

More detailed information on the structure and phase composition of the milled samples was obtained from Mössbauer spectroscopy data. Figure. 2 shows the Mössbauer spectra of as-melt-spun and milled samples and the corresponding hyperfine magnetic field distribution functions $P(H)$. The spectrum of the as-melt-spun state only shows a poorly resolved doublet corresponding to the amorphous phase, which is known to be paramagnetic at room temperature for any Zr content.[25] After 5 min of milling, a sextet with asymmetrically broadened lines is superposed to the doublet in the Mössbauer spectrum. Along with a 0–50 kOe low-field component corresponding to the amorphous phase, the $P(H)$ functions restored from Mössbauer spectra show a component at fields larger than 250 kOe, which stems from the bcc $\alpha$-Fe(Zr) solid solution. The contribution of the sextet increases with milling time. After 30 min of milling, the doublet almost disappears, indicating full crystallization of the amorphous phase, in good agreement with XRD results. An additional broad and flat middle-field component between 50 and 250 kOe can be clearly seen in the $P(H)$ functions of the milled samples (see Fig. 2), which can be assigned neither to the amorphous phase nor to the solid solution. It may be attributed to a strongly disordered $Fe_3Zr$ phase, which appears under thermally induced crystallization of amorphous $Fe_{90}Zr_{10}$[26,27]. However, the middle-field component is rather flat and uncharacteristic for any intermetallic compound and more likely results from Fe atoms having relatively large number of Zr atoms in their nearest neighborhood. This component cannot be also ascribed to the Fe atoms belonging to the boundaries of solid solution grains and being in contact with Zr segregations, since it was not observed under mechanical alloying in Fe-Zr system,[31] where strong segregation of Zr at Fe grain boundaries also took place. Therefore, 50–150 kOe component in Mössbauer spectra is related to Fe atoms in some disordered Zr-rich zones, which are presumably located near grain boundaries and arise as a result of extrusion of Zr atoms from forming grains of solid solution. However, the atomic structure of these zones and the way of their formation remain rather unclear and are the subjects of future investigations.

The saturation magnetization $\sigma_S$ shows a considerable increase with milling time (see Fig. 3). Such an increase in $\sigma_S$ means that chemical binding between Fe and Zr diminishes, Zr atoms segregate, and Zr-rich zones arise. It is consistent with the above conclusions made from XRD and Mössbauer results. Therefore, high-energy ball milling of amorphous $Fe_{90}Zr_{10}$ results in its crystallization into supersaturated nanocrystalline $\alpha$-Fe(Zr) with grains surrounded by Zr segregations.

### B. Crystallization under low-energy ball milling in Pulverizette-7 mill and cryomilling

To analyze the influence of milling intensity and local heating on the crystallization behavior, low-energy milling in a Pulverizette-7 was carried out in two temperature regimes: at room temperature (≈295 K, marked *RT* in figures) and at a reduced temperature of 245 K (marked *cold*). For cryomilling experiments (marked *cryo*), the vial was placed into liquid nitrogen, cooled for 10 min before milling, and subsequently kept under these conditions for the entire milling time. Thus, the temperature of the vial walls was constantly kept close to 77 K.

XRD patterns of samples room-temperature (RT) and cold milled for 30 min (Fig. 4) exhibit peaks corresponding to the bcc $\alpha$-Fe(Zr) solid solution identical to those obtained for high-energy milling. Some traces of the initial halo corresponding to the amorphous phase still remain in the pattern, indicating an incomplete crystallization of $Fe_{90}Zr_{10}$. However, these differences in crystallization kinetics can be easily explained, considering that the crystallization process should be slower under lower milling intensity. The sample after 30 min of cryomilling reveals a similar XRD pattern, with the crystallization process being far from completion.

Mössbauer spectra of the samples RT and cold milled for 30 min (Fig. 5) are similar to those of the sample milled in the AGO-2 mill for 5 min, with slight differences in the contribution of the paramagnetic doublet (resulting from the differences in power intensities). The $P(H)$ functions restored

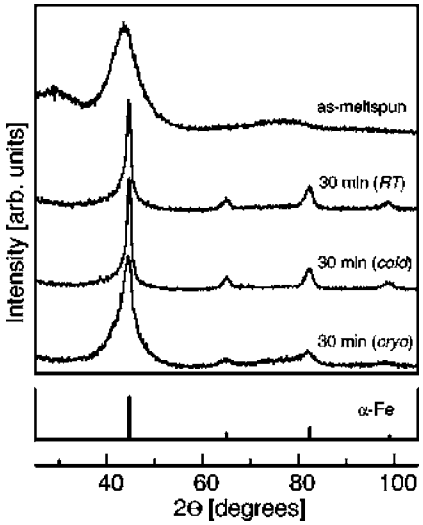


FIG. 4. XRD patterns of samples after low-energy milling and cryomilling. The standard XRD pattern of $\alpha$-Fe is shown below.

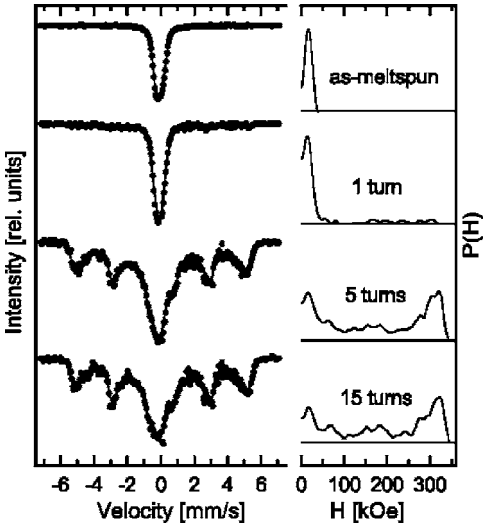


FIG. 6. Mössbauer spectra and corresponding hyperfine magnetic-field distribution functions of samples after high-pressure torsion.

from the spectra show the same set of components as for high-energy milling, namely, a low-field component of the amorphous phase, a high-field one stemming from the solid solution, and an intermediate broad component corresponding to disordered Zr-rich zones. Another difference with respect to high-energy milling is a lower concentration of the solid solution leading up to a sharper form of sextet lines, which plausibly arises from competition between mechanical disordering and thermal relaxation processes.

The Mössbauer spectrum of the cryomilled sample also shows the appearance of a sextet corresponding to $\alpha$-Fe(Zr) solid solution but of lower intensity and with broader lines. Such broadening can arise either from a higher concentration of a solid solution or because of its larger inhomogeneity due to slowed down relaxation processes at low temperatures.

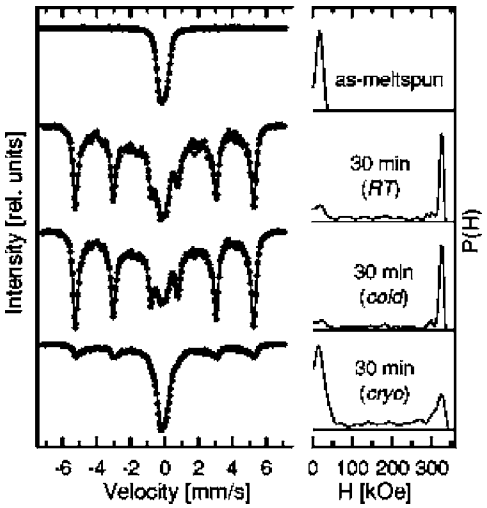


FIG. 5. Mössbauer spectra and corresponding hyperfine magnetic-field distribution functions of samples after low-energy milling and cryomilling.

### C. Crystallization under high-pressure torsion

Only Mössbauer measurements were carried out for the samples treated by high-pressure torsion, as reliable XRD investigations were difficult due to an extremely small sample area (of a few square millimeters). First, traces of crystallization are observed after one turn of the anvil. A small deviation of the Mössbauer spectrum from the nonresonance level can be observed for velocities outside the amorphous doublet range (see Fig. 6). After five turns, crystallization becomes explicit, and a well-pronounced sextet, as well as a broad intermediate component in the $P(H)$ function, arises as observed for ball-milled samples. The spectrum and corresponding $P(H)$ function after 15 turns are similar. Sextet lines for these samples are considerably broader than for the high- and low-energy milled ones, resembling those of the cryomilled sample. Such a difference points to the increase in Zr concentration of the solid solution obtained under lower temperatures with respect to that obtained under high-energy ball milling. Thus, high-pressure torsion induces crystallization of the amorphous ribbons in the same way as ball milling does. Supersaturated $\alpha$-Fe(Zr) solid solution is formed, as well as Zr-enriched regions, which give rise to the middle-field part in the Mössbauer spectra.

## IV. DISCUSSION

As it was mentioned above, milling-induced crystallization can be considered as a result of two simultaneous processes, namely, mechanical deformation of a material and its local heating due to ball collisions. Crystallization due to impurity incorporation was excluded in our case, as an oxygen content $<100$ ppm and a Fe impurity concentration $<0.5$ at. %, stemming from the debris of the milling tools, were detected by means of carrier-gas hot-extraction and energy dispersive x-ray analysis, respectively.

The drastic difference between crystallization products obtained under ball [milling supersaturated $\alpha$-Fe(Zr) solid solution+Zr segregations] and thermal annealing ($\alpha$-Fe $+Fe_3Zr$, Refs. 26 and 27), as well as the strongly nonequilibrium state of $\alpha$-Fe(Zr), indicates the important role of mechanical deformation in MIC. Similar differences in products were also observed in Ref. 14 for Al-based metal glasses. To a first approximation, it can be concluded that mechanical deformation is the primary reason for MIC, unlike crystallization induced by annealing. However, the basic role of mechanical deformation cannot be established unambiguously based on the difference in crystallization products. Local heating in a mill can also induce crystallization while mechanical deformation at the same time just disorders already formed products. In the latter case, nonequilibrium phases would also arise as a result of milling process. The temperature of the balls in the AGO-2 mill under the applied milling conditions reaches 400 °C according to calorimetric measurements.[13] Therefore, local temperatures at points of ball collisions can be remarkably higher and, taking into account that the crystallization temperature of $Fe_{90}Zr_{10}$ is about 660 °C (Ref. 21), can become sufficient to initiate thermal crystallization.

On the other hand, the study and comparison of evolution of amorphous $Fe_{90}Zr_{10}$ under different milling conditions and high-pressure torsion allow the establishment of the roles of mechanical deformation and local heating in the MIC process. Ball milling in the high-energy AGO-2 mill results in the formation of supersaturated $\alpha$-Fe(Zr) solid solution with Zr segregations at grain boundaries. Low-energy ball milling in the Pulverizette-7 mill, where local temperatures are lower than in AGO-2 mill and were theoretically estimated to be about 300–400 °C, reveals an identical crystallization behavior. MIC under cryomilling is also similar to MIC under room temperature. The only difference is that the solid solution formed under cryomilling is further away from thermodynamic equilibrium. High-pressure torsion of amorphous ribbons also results in the crystallization of amorphous $Fe_{90}Zr_{10}$ ribbons, with the same crystallization behavior and products.

No difference in the crystallization process between high-energy ball milling and high-pressure torsion, except slight changes in the concentration of the solid solution, was detected in spite of the large differences in local heating of the samples. Such an observation unambiguously demonstrates the nonthermal character of MIC, with mechanical deformation being the primary reason for crystallization. First theoretical approaches for the description of similar mechanically induced phase transformations (demixing of solid solutions, etc.) during severe plastic deformations were proposed.[32]

Local heating occurring under high-energy ball milling only accelerates the relaxation processes of products, and a slight shift of the formed solid solution towards equilibrium state takes place. Heating may also alter the crystallization kinetics, which seems to differ for different milling conditions, as the temperature has a slight effect on the kinetics of mechanical alloying,[33] but it is determined in a greater degree by the power intensity of a mill, and the role of thermal factors in the kinetics of MIC remains virtually insufficient. However, the influence of local heating may become more pronounced for low-melting amorphous alloys, when the temperature in the mill is close to the melting point. Further investigations in this field are still required to be carried out.

## V. CONCLUSION

Amorphous $Fe_{90}Zr_{10}$ ribbons crystallize under ball milling and high-pressure torsion into a supersaturated $\alpha$-Fe(Zr) solid solution with grain sizes less than 20 nm and a maximum Zr concentration of about 3 at.%. Residual Zr atoms (not included into solid solution grains) form grain-boundary segregations. Impurity incorporation has been excluded as a possible reason of the crystallization process. The crystallization product of the ball milling process strongly differs from that obtained under thermal annealing of $Fe_{90}Zr_{10}$ amorphous ribbons. On the other hand, very similar crystallization behaviors were found for high- and low-energy millings, cryomilling, and high-pressure torsion despite considerable differences in the rise of local temperature during mechanical treatment. This similarity indicates that mechanical deformation is the primary reason for milling-induced crystallization. Local heating only plays a minor role in the process, resulting in a slight shift of the formed solid solution towards equilibrium state owing to accelerated relaxation processes at increased local temperatures.

## ACKNOWLEDGMENTS

This work was supported by the Korea Science and Engineering Foundation (KOSEF), Project No. F01-2004-10395-0, through the Research Center for Machine Parts and Materials Processing (ReMM) of the University of Ulsan. We are thankful to Kim Do-Hyang and Park Jin-Man from Yonsei University (Korea) for the preparation of melt-spun samples.

*Corresponding author. FAX: 7-3412-250614. Electronic address: povst@fnms.fti.udm.ru

[1] C. C. Koch, O. B. Cavin, G. McKamey, and J. O. Scarborough, Appl. Phys. Lett. **43**, 1017 (1983).

[2] L. Schultz, Mater. Sci. Eng. **97**, 15 (1988).

[3] J. Eckert, L. Schultz, and K. Urban, Mater. Sci. Eng., A **134**, 1389 (1991).

[4] R. B. Schwarz, R. R. Petrich, and C. K. Saw, J. Non-Cryst. Solids **76**, 281 (1985).

[5] J. Eckert, L. Schultz, E. Hellstern, and K. Urban, J. Appl. Phys. **64**, 3224 (1988).

[6] H. Bakker, G. F. Zhou, and H. Yang, Mater. Sci. Forum **179-181**, 47 (1995).

[7] C. Bansal, B. Fultz, and W. L. Johnson, Nanostruct. Mater. **4**, 919

(1994).
[8] M. L. Trudeau, Appl. Phys. Lett. **64**, 3661 (1994).
[9] B. Huang, R. J. Perez, P. J. Crawford, A. A. Sharif, S. R. Nutt, and E. J. Lavernia, Nanostruct. Mater. **5**, 545 (1995).
[10] J. Xu and M. Atzmon, Appl. Phys. Lett. **73**, 1805 (1998).
[11] M. Pekala, M. Jachimowicz, V. I. Fadeeva, and H. Matyja, J. Non-Cryst. Solids **287**, 360 (2001).
[12] R. M. Davis, B. McDermott, and C. C. Koch, Metall. Trans. A **19A**, 2867 (1988).
[13] Y. S. Kwon, K. B. Gerasimov, and S. K. Yoon, J. Alloys Compd. **346**, 276 (2002).
[14] Y. He, G. J. Shiftlet, and S. J. Poon, Acta Metall. Mater. **43**, 83 (1995).
[15] D. R. Maurice and T. H. Courtney, Metall. Trans. A **21A**, 289 (1990).
[16] X. J. Gu, F. Ye, F. Zhou, and K. Lu, Mater. Sci. Eng., A **278**, 61 (2000).
[17] B. Yao, S. E. Liu, L. Liu, W. H. Su, and Y. Li, J. Appl. Phys. **90**, 1650 (2001).
[18] W. H. Jiang and M. Atzmon, Scr. Mater. **54**, 333 (2006).
[19] J. J. Lewandowski and A. L. Greer, Nat. Mater. **5**, 15 (2006).
[20] N. Burgio, A. Iasonna, M. Magini, S. Martelli, and F. Padella, Nuovo Cimento D **13**, 459 (1991).
[21] A. W. Weeber and H. Bakker, Physica B **153**, 93 (1988).
[22] S. E. Lee, H. Y. Ra, T. H. Yim, and W. T. Kim, Mater. Sci. Forum **179-181**, 121 (1995).
[23] R. Pizarro, J. S. Garitaonandia, F. Plazaola, J. M. Barandiaran, and J. M. Greneche, J. Phys.: Condens. Matter **12**, 3101 (2000).
[24] K. M. Unruh and C. L. Chien, Phys. Rev. B **30**, 4968 (1984).
[25] H. Tange, Y. Tanaka, M. Goto, and K. Fukamichi, J. Magn. Magn. Mater. **81**, L243 (1989).
[26] M. Ghafari, U. Gonser, H. G. Wagner, and M. Naka, Nucl. Instrum. Methods Phys. Res. **199**, 197 (1982).
[27] L. F. Kiss, G. Huhn, T. Kemeny, J. Balogh, and D. Kaptas, J. Magn. Magn. Mater. **160**, 229 (1996).
[28] E. V. Voronina, N. V. Ershov, A. L. Ageev, and Yu. A. Babanov, Phys. Status Solidi B **160**, 625 (1990).
[29] I. V. Povstugar and P. Yu. Butyagin, J. Mater. Sci. **39**, 5461 (2004).
[30] E. P. Yelsukov and G. A. Dorofeev, J. Mater. Sci. **39**, 5071 (2004).
[31] I. V. Povstugar, P. Yu. Butyagin, G. A. Dorofeev, and E. P. Elsukov, Colloid J. **64**, 201 (2002).
[32] V. V. Kondrat'ev and V. L. Gapontsev, Phys. Met. Metallogr. **94**, S131 (2002).
[33] C. H. Lee, M. Mori, T. Fukunaga, and U. Mizutani, Jpn. J. Appl. Phys., Part 1 **29**, 540 (1990).